JOURNAL OF GEOPHYSICAL RESEARCH, VOL. 91, NO. D9, PAGES 9857–9864, AUGUST 20, 1986

Infrared Radiation Models for Atmospheric Methane

R. D. CESS, D. P. KRATZ, S. J. KIM,[1] AND J. CALDWELL

Laboratory for Planetary Atmospheres Research, State University of New York, Stony Brook

Mutually consistent line-by-line, narrow-band and broad-band infrared radiation models are presented for methane, a potentially important anthropogenic trace gas within the atmosphere. Comparisons of the modeled band absorptances with existing laboratory data produce the best agreement when, within the band models, spurious band intensities are used which are consistent with the respective laboratory data sets, but which are not consistent with current knowledge concerning the intensity of the infrared fundamental band of methane. This emphasizes the need for improved laboratory band absorptance measurements. Since, when applied to atmospheric radiation calculations, the line-by-line model does not require the use of scaling approximations, the mutual consistency of the band models provides a means of appraising the accuracy of scaling procedures. It is shown that Curtis-Godson narrow-band and Chan-Tien broad-band scaling provide accurate means of accounting for atmospheric temperature and pressure variations.

1. INTRODUCTION

While there is a general consensus that anthropogenically induced increases in atmospheric CO_2 could impact the earth's future climate, more recently it has become apparent that numerous other anthropogenic trace gases might collectively be of comparable importance [e.g., *WMO*, 1982; *Ramanathan et al.*, 1985]. This in turn has emphasized the need for improved trace-gas radiative transfer models. Towards this goal, one purpose of the present paper is to develop accurate infrared band models for methane which is a potentially important anthropogenic greenhouse gas [*Ramanathan et al.*, 1985].

Moreover, there currently is a great deal of interest in evaluating errors introduced through the use of simplified band models [*WMO*, 1984], and a second purpose of the present paper is to use the ν_4 band of CH_4 (centered at 1306 cm^{-1}) as an illustrative infrared band for the purpose of intercomparing a hierarchy of band models.

For the atmospheric application of a band model there are two issues involved: the applicability of the band model to accurately characterize the total band absorptance for a homogeneous gas (i.e., constant temperature and pressure), and the validity of associated scaling approximations which must be invoked when the band model is employed for atmospheric applications, where temperature and pressure vary. The second item is of particular importance with respect to broad-band models. Although several broad-band scaling approximations have been suggested [*Chan and Tien*, 1969; *Cess and Wang*, 1970; *Edwards and Morizumi*, 1970], there has not been a definitive examination of their accuracies.

The specific strategy of this paper is as follows. A reference line-by-line calculation will first be discussed, followed by the presentation of narrow-band and broad-band models which are tuned, for a homogeneous gas, to the line-by-line model. Thus a hierarchy of band models is obtained which yield nearly identical homogeneous band absorptances. With reference to the line-by-line model, this affords a means of appraising the accuracy of scaling approximations for both the narrow-band and broad-band models when they are applied to atmospheric radiation calculations. In addition, there will be a brief discussion concerning pitfalls associated with the use of narrow-band models, together with an intercomparison of the present results with existing CH_4 infrared band models.

2. BAND MODELS

The line-by-line calculations employed both Voigt and Lorentz line shapes, a wavenumber integration interval of 5×10^{-4} cm^{-1}, and a wavenumber cutoff of 12 cm^{-1} (i.e., the spectral absorption coefficient includes the effects of all rotational lines within a 24 cm^{-1} range centered at the wavenumber of the absorption coefficient calculation). Both the integration interval and the cutoff were chosen on the basis of sensitivity studies, and for many applications it was found that larger intervals and smaller cutoffs were adequate.

The line locations and intensities were taken from a JPL data tape [*Orton and Robiette*, 1980], incorporating all CH_4 lines within the wavenumber interval of 1100 to 1700 cm^{-1}. The line intensities were renormalized to a total band intensity of 128 cm^{-2} atm^{-1} at 296 K for the ν_4 band [*Varanasi et al.*, 1983; *Chedin and Scott*, 1984]. The air-broadened Lorentz half-width per unit pressure, γ^0, was taken to be

$$\gamma^0(cm^{-1}\ atm^{-1}) = 0.06(296/T) \tag{1}$$

for all lines, based upon *Varanasi et al.* [1983], who obtained a coefficient of 0.063 (with a standard deviation of 0.003) for 77 lines within the wavenumber interval 1300–1353 cm^{-1}. Since the JPL data tape contains roughly 12,000 lines, this constitutes a rather extensive extrapolation, and it can only be emphasized that our current knowledge of line half-widths is meager at best.

Turning next to the narrow-band model, we have attempted regression fits to line-by-line calculations employing modified versions of both the *Goody* [1952] and *Malkmus* [1967] random band models; for present purposes the former proved to be the most useful. The transmittance $T_{\Delta\omega}$ for a given wavenumber interval $\Delta\omega$ is given by the Goody model as

$$T_{\Delta\omega} = \exp\{-(S_{\Delta\omega}m/\Delta\omega)[1 + (S_{\Delta\omega}m/\pi\bar{\gamma})]^{-1/2}\} \tag{2}$$

where m is the absorber amount, $S_{\Delta\omega}$ is the sum of the line intensities within the interval, and $\bar{\gamma}$ is defined by the relation

$$S_{\Delta\omega}\bar{\gamma} = C[\sum (\gamma_{JK}S_{JK})^{1/2}]^2 \tag{3}$$

[1]Now at National Space Science Data Center, NASA Goddard Space Flight Center, Greenbelt, Maryland.

Paper number 6D0257.
0148-0227/86/006D-0257$05.00

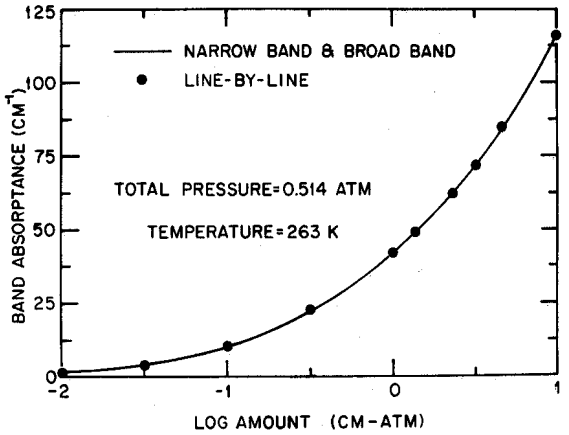

Fig. 1. Band absorptance comparisons for the line-by-line, narrow-band and broad-band models. The latter two are represented by a single curve, since there is no distinguishable difference between them. The methane amount refers to standard temperature.

where γ_{JK} and S_{JK} denote the individual line half-widths and line intensities, respectively, and the summation is over all lines within $\Delta\omega$. The spectroscopic data used here is the same as in the line-by-line calculations.

Conventionally the constant C is determined such that (2) is consistent with the limit of strong nonoverlapping lines [e.g., *Goody*, 1964], with the result that $C = 4/\pi$. This determination follows from the assumption that in the limit of strong nonoverlapping lines (square-root limit) the individual line absorptances are nonoverlapping, which produces the averaging expression given by (3). For conincident lines, however, (3) would be replaced by linear averaging, resulting in a smaller value for $\bar{\gamma}$. Thus if there are a significant number coincident or near-coincident lines, one would anticipate that $C < 4/\pi$.

For present purposes $\Delta\omega = 5$ cm^{-1}, with elaboration on this choice to be given later. The coefficient C appearing in (3) has been evaluated by performing a regression fit of (2) to the line-by-line calculations. This was done for total pressures ranging from 0.1 to 1 atm, for temperatures spanning 220 K to 300 K, and for a range of CH_4 amounts from 10^{-2} to 10 cm-atm at standard temperature. For these conditions there is no distinction between the use of either the Voigt or Lorentz line profiles in the line-by-line calculations, thus assuring consistency with (2) which is based upon a Lorentz profile. The regression fit produced $C = 0.753$, and a comparison of the narrow-band and line-by-line results is illustrated in Figure 1 for a temperature of 263 K and a total pressure of 0.514 atm, both of which correspond to average values for the atmospheric calculations of the following sections.

As just discussed, one would anticipate that $C < 4/\pi$ if coincident and near-coincident lines are a factor, which could indeed be the case due both to line splitting and the presence of a Q branch for the ν_4 band of CH_4. But to be more specific on this point we have reevaluated the line-by-line and Goody models adopting a procedure by which coincident and near-coincident lines are combined into a single equivalent line. This was accomplished by combining all lines which are located within a specified wavenumber interval of each other, taking this combination interval to be an arbitrary parameter.

These results are summarized in Table 1 for the conditions of Figure 1 together with a CH_4 mixing ratio of 1.75×10^{-6}. The important point is that while the line-by-line results are quite insensitive to the choice of wavenumber combination interval, there is a significant dependence for the Goody model. This suggests that much of the difference between the regression-determined $C = 0.753$ and the conventional $C = 4/\pi = 1.273$ might be attributable to coincident and near-coincident lines. Recall that such lines should be linearly summed, as is effectively done in the line-by-line model, instead of using the averaging procedure of (3). But the value of C also depends upon other factors as later discussed.

With respect to a broad-band model, a hybrid version of those proposed by *Cess and Ramanathan* [1972], and *Ramanathan* [1976], is adopted, for which the total band absorptance is expressed as

$$A = 2A_0 \ln\left[1 + \sum\left(\frac{u}{D + \sqrt{E + u(1 + 1/\beta)}}\right)\right] \tag{4}$$

where $E = (2 - D)^2$, $u = Sm/A_0$ with S the total band intensity, β is proportional to the ratio of the mean line half-width to mean line spacing, and the summation refers to the overlapping $^{12}CH_4$ and $^{13}CH_4$ isotope bands. For $D = 2$ this reduces to the formulation of *Cess and Ramanathan* [1972], while for $D = 0$ it coincides with that of *Ramanathan* [1976].

The quantities D, A_0 and β have been determined from a regression fit to the line-by-line calculations, and here it was necessary to additionally evaluate the temperature dependence of A_0. This resulted in $D = 1.06$ together with

$$A_0(\text{cm}^{-1}) = 68.2(T/300)^{0.858} \tag{5}$$

$$\beta = 0.211P(300/T) \tag{6}$$

where P is the total pressure (atm). The temperature dependence of β is that of (1) since $\beta = 4\gamma^0 P/\delta$ [*Ramanathan*, 1976], where δ is the mean line spacing. In the absence of line splitting δ would be 5.1 cm^{-1} (which is the multiplet spacing), resulting in $\beta = 0.046$ at 300 K. The larger value of β given by (6) is consistent with $\delta < 5.1$ cm^{-1} due to line splitting. The dependence of A_0 upon temperature is in contrast to the often-used square-root temperature dependence, as determined by *Edwards and Menard* [1964*a*] for the molecular model of a rigid rotator and harmonic oscillator. But departures from a square-root dependence have also been noted by *Brosmer and Tien* [1985] for CH_4, and by *Ramanathan and Dickinson* [1979] for O_3. In fact *Edwards and Menard* [1964*a*] found a linear temperature dependence for a simplified nonrigid rotator model.

The 1100–1700 cm^{-1} line-by-line and narrow-band models incorporate absorption due not only to the ν_4 band, but also that due to the weak ν_2 fundamental band located at roughly 1550 cm^{-1}. To achieve consistency between these models and the broad-band model, we simply employ within the broad-band model a band intensity which is the sum of that due to the ν_2 and ν_4 bands. For the present ν_4 band intensity of 128 cm^{-2} atm^{-1} at 296 K, the ν_2 plus ν_4 intensity is 129.4 cm^{-2} atm^{-1}.

A comparison of the broad-band model with the 263 K and 0.514 atm line-by-line results is shown in Figure 1, where a

TABLE 1. Comparison of CH_4 Total Band Absorptances (cm^{-1}) for a CH_4 Mixing Ratio of 1.75×10^{-6}, $P = 0.514$ and $T = 263$ K

Combination Interval, cm^{-1}	Line-by-Line Model	Goody Model
0	48.86	56.29
0.01	48.86	55.52
0.03	48.69	53.03
0.05	48.08	49.03

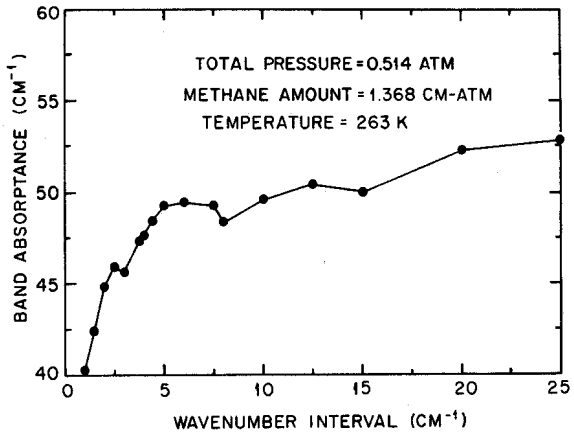

Fig. 2. Band absorptance, evaluated from the narrow-band model, as a function of wavenumber interval $\Delta\omega$. The methane amount is the same as for the atmospheric column and refers to standard temperature.

single curve is used to denote both the narrow-band and broad-band models since there is no distinguishable difference between them.

Before proceeding it is necessary to elaborate on several aspects of the narrow-band model. Consider first the present choice of $\Delta\omega = 5$ cm^{-1}. As pointed out by *Kiehl and Ramanathan* [1983] for CO_2, significant errors can occur if one employs overly large spectral intervals. This is due to the statistics of the band structure, as manifested by the averaging procedure of (3), being variable throughout the band. One way of minimizing this effect is to choose small intervals with the hope that this will produce near-uniform statistics within each interval. But if the intervals are too small there will not be a sufficient number of lines within the intervals to yield meaningful statistics.

Ideally, one would anticipate that there should be an interval range over which the computed band absorptance is nearly invariant to the choice of interval size, with the intervals being sufficiently large to contain a statistically meaningful number of lines, but at the same time sufficiently small so that (3) produces meaningful statistical averages. However, as illustrated in Figure 2, CH_4 does not produce such a clearly defined range of intervals. The small plateau for $\Delta\omega$ varying from roughly 5 to 8 cm^{-1} was the sole motivation for our choice of $\Delta\omega = 5$ cm^{-1}. The rapid change in band absorptances for $\Delta\omega < 5$ cm^{-1} is a consequence of the multiplet spacing being roughly 5 cm^{-1}, such that $\Delta\omega$ smaller than this value produces spectral gaps.

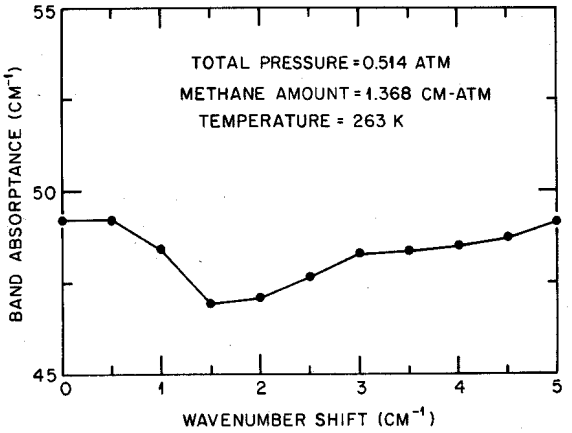

Fig. 3. Band absorptance, evaluated from the narrow-band model, as a function of the shift in wavenumber interval for $\Delta\omega = 5$ cm^{-1}. The methane amount is the same as for the atmospheric column and refers to standard temperature.

TABLE 2. Summary of Experimental Conditions for the Laboratory Measurements of *Gryvnak et al.* [1976]

Sample Number	Total Pressure, atm	Partial Pressure, atm	Wavenumber Interval, cm^{-1}
4	1.00	0.1000	1188–1400
5	1.00	0.0500	1210–1400
6	1.00	0.0250	1210–1400
7	0.30	0.0300	1210–1385
8	0.30	0.0150	1210–1385
9	0.30	0.0075	1210–1385
10	0.10	0.0100	1210–1385
11	0.10	0.0050	1260–1370
12	0.10	0.0025	1260–1370
13	0.03	0.0030	1260–1370

In all cases the cell length was 10.2 cm, while gas temperatures ranged from 302 to 304 K.

The regression determination of C is somewhat insensitive to $\Delta\omega$ for $\Delta\omega$ ranging from 5 cm^{-1} to 15 cm^{-1} ($C = 0.753$ for $\Delta\omega = 5$ cm^{-1} and $C = 0.715$ for $\Delta\omega = 15$ cm^{-1}). But for larger $\Delta\omega$ the value of C changes considerably ($C = 0.571$ for $\Delta\omega = 25$ cm^{-1}), and with this is a simultaneous degradation of the regression fit.

A second issue concerns the location of the wavenumber intervals. Figure 3 illustrates a band absorptance calculation in which the locations of the intervals ($\Delta\omega = 5$ cm^{-1}) were progressively shifted. For example, a wavenumber shift of 0 (or 5 cm^{-1}) corresponds to interval locations of 1200–1205 cm^{-1}, etc., while for a wavenumber shift of 1 cm^{-1} these are 1201–1206, etc. In Figure 3 this produces a 5 percent variation in band absorptance, an effect which is again related to a variation in band statistics within the 5 cm^{-1} intervals, as the interval positions are shifted. Comparable variability exists for $\Delta\omega = 10$ cm^{-1}.

3. Comparison With Laboratory Data

Although it is obviously advisable to compare model calculated band absorptances with laboratory data, such data [*Burch and Williams*, 1962; *Edwards and Menard*, 1964*b*; *Gryvnak et al.*, 1976] contain inherent inconsistencies in band intensity, with the inferred 296 K intensities being 171 cm^{-2}

TABLE 3. Comparison of Measured and Calculated Band Absorptances (cm^{-1})

Sample Number	*Gryvnak et al.* [1976]	Line-by-Line Model
4	50.06	49.65 (−0.8)
5	33.99	33.97 (−0.1)
6	22.77	22.18 (−2.6)
7	18.56	18.89 (+1.8)
8	12.33	12.46 (+1.1)
9	7.20	7.68 (+6.6)
10	7.41	7.02 (−5.3)
11	3.60	3.80 (+5.6)
12	2.52	2.31 (−8.3)
13	2.26	1.91 (−15.5)

The band intensity employed within the line-by-line model is 144 cm^{-2} atm^{-1} at 296 K, and the wavenumber intervals are those listed in Table 2. The numbers in parentheses denote the percentage differences from the Gryvnak et al. values.

TABLE 4. Comparison of Measured and Calculated Band Absorptances (cm^{-1})

Burch and Williams [1962]	Narrow-Band Model	
	$S = 171$ cm^{-2} atm^{-1}	$S = 128$ cm^{-2} atm^{-1}
290	295 (+1.7)	281 (−3.1)
238	231 (−2.9)	218 (−8.4)
77.3	83.3 (+7.8)	72.6 (−6.1)
45.5	47.9 (+5.1)	41.7 (−8.4)
20.2	17.7 (−12.4)	15.3 (−24.3)
2.78	2.46 (−11.5)	1.86 (−33.1)
2.20	2.26 (+2.7)	1.74 (−20.9)

The band intensities employed within the narrow-band model refer to 296 K. The numbers in parentheses denote the percentage differences from Burch and Williams' values.

atm^{-1} [*Burch and Williams*, 1962], 185 cm^{-2} atm^{-1} [*Edwards and Menard*, 1964*b*], and 144 cm^{-2} atm^{-1} [*Gryvnak et al.*, 1976], all of which are in excess of the currently accepted value of 128 cm^{-2} atm^{-1} [*Varanasi et al.*, 1983; *Chedin and Scott*, 1984]. For purposes of a tentative comparison, line-by-line calculations have been performed for conditions corresponding to the Gryvnak et al. data, but with our line intensities being renormalized to their inferred band intensity of 144 cm^{-2} atm^{-1}.

The Gryvnak et al. data comprise 10 measurements of the band absorptance for the experimental conditions summarized in Table 2. In contrast to atmospheric applications, self broadening is of some modest importance, and the self-broadened half-width was taken to be [*Varanasi et al.*, 1973]

$$\gamma^0(\text{cm}^{-1}\ \text{atm}^{-1}) = 0.083(296/T)^{0.8} \quad (7)$$

The line-by-line calculations were performed with both Voigt and Lorentz line profiles; only for sample 13 was there a noticeable difference, with the Voigt profile producing a band absorptance of 1.91, as opposed to 1.79 for the Lorentz profile. Comparison with the Gryvnak et al. data is shown in Table 3, and for the most part the agreement is reasonable.

It is worth noting that the Gryvnak et al. data do not constitute total band absorptance measurements, due to use of the rather narrow spectral intervals as summarized in Table 2. Utilizing the narrow-band model of the present study, we estimate that total band absorptances (1100–1700 cm^{-1}) would be from 3 percent (sample 6) to 21 percent (sample 11) larger than those summarized within Table 3.

At this juncture it is useful to employ the narrow-band model to illustrate a curious feature, just alluded to with respect to Table 3, concerning existing band absorptance data. As previously discussed, *Burch and Williams* [1962] have performed band absorptance measurements from which they inferred a band intensity of 171 cm^{-2} atm^{-1} at 296 K. These measurements refer to the wavenumber interval 1100 to 1535 cm^{-1} which excludes the weak ν_2 fundamental band. To be consistent with their measurements, we have performed additional narrow-band computations for which the wavenumber interval 1535 to 1700 cm^{-1} has been excluded.

Edwards and Menard [1964*b*] conveniently summarize certain of the Burch and Williams data, and these are listed in Table 4 together with the corresponding calculations employing the narrow-band model in conjunction with both the currently adopted band intensity and that inferred by Burch and Williams. A single band absorptance contained within the Edwards and Menard summary, corresponding to conditions for which there is a departure from a Lorentz line shape due to Doppler broadening, has been excluded.

The curious point is that use of the erroneously high band intensity of Burch and Williams produces much better agreement between the narrow-band model and the laboratory data. A similar conclusion applies to Table 3, since if we had there employed $S = 128$ cm^{-2} atm^{-1} within the line-by-line model, rather than $S = 144$ cm^{-2} atm^{-1} as inferred by *Gryvnak et al.* [1976], the agreement between the line-by-line calculations and the Gryvnak et al. data would be degraded. This raises the possibility (P. Varanasi, private communication, 1985) that both sets of band absorptance data contain systematic errors in the determination of the CH_4 partial pressure.

4. Scaling Approximations

The virtual equivalence of the narrow-band and broad-band models with the line-by-line calculations (Figure 1) conveniently allows an evaluation of nonhomogeneous band-model scaling approximations. For this purpose total band absorptances will be compared for the atmospheric column extending from the surface to 25 km, employing the midlatitude summer atmosphere of *McClatchey et al.* [1971]. Since we are focusing upon the examination of radiative transfer approximations, overlap with water vapor and clouds will be ignored. The CH_4 volumetric mixing ratio is simplistically assumed to be invariant with altitude and is taken to be 1.75×10^{-6}.

Curtis-Godson scaling constitutes the conventional scaling approximation for use with narrow-band models, and that described by *Rodgers and Walshaw* [1966] is adopted here. Since this scaling is exact in both the weak-line and strong-line limits, it would not be useful to test Curtis-Godson scaling by employing an atmospheric gas which is close to either of these limits. For example, the relevant bands of atmospheric CO_2 are primarily in the strong-line limit. Atmospheric CH_4, however, is an excellent choice, since for the present atmospheric abundance it is well removed from either limit, as is illustrated in Figure 4 for an equivalent homogeneous atmosphere.

An additional procedure for treating nonhomogeneous paths is also described by *Rodgers and Walshaw* [1966]. They employed the line intensity distribution of the Goody random band model, and they assumed that all lines within each spectral interval could be replaced by a single effective line for

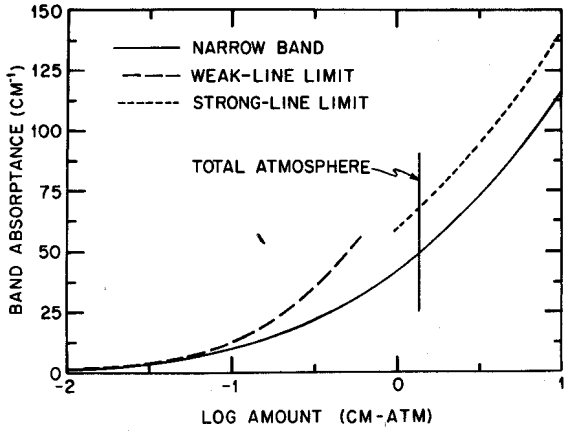

Fig. 4. Comparison of the narrow-band model with its weak-line and strong-line limits. The methane amount refers to standard temperature, and the methane amount for the present total atmospheric column is 1.368 cm atm.

TABLE 5. Comparisons of Atmospheric (0 to 25 km) CH_4 Total Band Absorptance for a CH_4 Mixing Ratio of 1.75×10^{-6}

Model	Scaling	Band Absorptance, cm^{-1}	
		Homogeneous	Nonhomogeneous
Line-by-line		48.86	47.48
Narrow-band	Rodgers-Walshaw	49.20	48.09
Narrow-band	Curtis-Godson	49.20	48.67
Broad-band	Chan-Tien	49.25	48.50
Broad-band	Edwards-Morizumi	49.25	49.09
Broad-band	Cess-Wang	49.25	50.23

The homogeneous atmosphere ($P = 0.514$ atm and $T = 263$ K) contains the same CH_4 amount as the nonhomogeneous atmosphere.

which the half-width is $\bar{\gamma}$ as defined by (3). The resulting expression for the spectral transmittance is

$$T_{\Delta\omega} = \exp\left[-\frac{1}{\Delta\omega}\int_{-\infty}^{\infty}\frac{\tau}{1+\tau}\,d\omega\right] \tag{8}$$

where τ is defined by the path-length integral

$$\tau = \frac{1}{\pi}\int\frac{S_{\Delta\omega}\bar{\gamma}}{\bar{\gamma}^2+\omega^2}\,dm \tag{9}$$

For homogeneous paths this reduces to the Goody random band model or, with $C = 0.753$ within (3), to the narrow-band model of the prior section.

With respect to broad-band models, there have been three suggested scaling procedures [*Chan and Tien*, 1969; *Cess and Wang*, 1970; *Edwards and Morizumi*, 1970], all of which produce scaled broad-band parameters $\tilde{A}_0$ and $\tilde{\beta}$. For Chan-Tien scaling

$$\tilde{A}_0 = 1/m\int A_0(T)\,dm \tag{10}$$

$$\tilde{\beta} = 1/m\int \beta(T, P)\,dm \tag{11}$$

This expression for $\tilde{A}_0$ is also utilized in Edwards-Morizumi scaling, but (11) is replaced by

$$\tilde{\beta} = \frac{1}{\tilde{A}_0 m}\int \beta(T, P)A_0(T)\,dm \tag{12}$$

For Cess-Wang scaling, $\tilde{\beta}$ is given by (12), while

$$\tilde{A}_0 = A_0(T_{\max}) \tag{13}$$

where $T_{\max}$ denotes the maximum temperature within the path-length integration. While all three scaling procedures also give a temperature-scaled band intensity, this is not relevant to the present problem, since in mass units the intensity of a fundamental band is independent of temperature.

TABLE 6. Ratio of the Atmospheric CH_4 Band Absorptance for the Nonhomogeneous Atmosphere to That for the Homogeneous Atmosphere

Model	Scaling	Ratio
Line-by-line		0.972
Narrow-band	Rodgers-Walshaw	0.977 (0.5)
Narrow-band	Curtis-Godson	0.989 (1.7)
Broad-band	Chan-Tien	0.985 (1.3)
Broad-band	Edwards-Morizumi	0.997 (2.6)
Broad-band	Cess-Wang	1.020 (4.9)

See Table 5. The numbers in parentheses denote the percentage difference from the line-by-line value.

TABLE 7. Comparison of Model Calculations for the Change in Infrared Flux Due to the Presence of CH_4 With a Mixing Ratio of 1.75×10^{-6}

Model	Flux Reduction, W/m^2		
	Top	Tropopause	Surface
Line-by-line	4.88	4.68	6.38
Narrow-band (Curtis-Godson)	4.89 (0.2)	4.62 (−1.3)	6.37 (−0.2)
Broad-band (Chan-Tien)	4.92 (0.8)	4.64 (−0.9)	6.44 (0.9)
Broad-band (Edwards-Morizumi)	4.97 (1.8)	4.66 (−0.4)	6.46 (1.3)
Broad-band (Cess-Wang)	5.07 (3.9)	4.73 (1.1)	6.54 (2.5)

The respective scaling approximations are given in parentheses; the numbers in parentheses denote the percentage differences from the line-by-line values.

Total band absorptances for the atmospheric column (0 to 25 km) are summarized in Table 5, employing all of the above discussed narrow-band and broad-band scaling procedures, together with a reference line-by-line calculation which does not necessitate scaling. These refer to the column labeled "nonhomogeneous." The differences between the tabulated values contain not only differences due to the scaling approximations, but also small differences which exist between the line-by-line, narrow-band and broad-band models. These differences are illustrated by the tabulated band absorptance values for the equivalent homogeneous atmosphere, and to remove this small effect the nonhomogeneous band absorptances have been ratioed to those for the equivalent homogeneous atmosphere. These results are summarized in Table 6. With the possible exception of Cess-Wang scaling, the various scaling procedures are in excellent agreement with the line-by-line result.

5. Atmospheric Flux Comparisons

To facilitate a more direct intercomparison of atmospheric radiation models, we consider the effect of CH_4 upon the net infrared flux at the surface, at the tropopause (13 km), and at the top of the atmosphere (25 km). The model atmosphere of the previous section is adopted, again ignoring overlap with water vapor and clouds and utilizing the mid-latitude summer atmosphere.

Letting $\Delta F(z)$ denote the change in net infrared flux at altitude z (taken as positive for a reduction in net upward flux), the formulation employed in the present study is

$$\Delta F(z) = \pi B_\omega(T_0)A[(z_0 - z)/\mu] - \pi\int_0^z A[(z - z')/\mu]\,dB_\omega - \pi\int_z^{z_0} A[(z' - z)/\mu]\,dB_\omega \tag{14}$$

where $A(z)$ is the atmospheric absorptance, T_0 and z_0 refer to the top of the atmosphere, $B_\omega(T)$ is the black-body intensity, and μ is the cosine of the zenith angle. Hemispherical averaging was performed through use of an 8-point Gaussian quadrature. This expression differs from that used by *Kiehl and Ramanathan* [1983] solely through an integration by parts.

As written, (14) applies directly to the broad-band model

TABLE 8. Comparison of Model Calculations for the Change in Infrared Flux Due to an Increase in CH_4 Mixing Ratio From 1.75×10^{-6} to 3.5×10^{-6}

Model	Flux Reduction, W/m²		
	Top	Tropopause	Surface
Line-by-line	1.78	1.78	2.40
Narrow-band (Curtis-Godson)	1.80 (1.1)	1.79 (0.6)	2.42 (0.8)
Broad-band (Chan-Tien)	1.85 (3.9)	1.85 (3.9)	2.56 (6.7)
Broad-band (Edwards-Morizumi)	1.86 (4.5)	1.86 (4.5)	2.57 (7.1)
Broad-band (Cess-Wang)	1.94 (9.0)	1.91 (7.3)	2.62 (9.0)

The respective scaling approximations are given in parentheses; the numbers in parentheses denote the percentage differences from the line-by-line values.

with $B_\omega(T)$ evaluated at the band center (1306 cm^{-1}). For the narrow-band model it applies to the individual $\Delta\omega$ intervals, and for the line-by-line calculations it is a monochromatic expression. Flux reductions due to present methane (1.75×10^{-6} ppv), and for a doubling of this value, are given in Tables 7 and 8 respectively, for the present narrow-band and broad-band models together with reference line-by-line calculations. As in the previous section, Voigt and Lorentz line shapes produce identical line-by-line results.

Differences between the band models and the line-by-line calculations tend to be consistent with the prior section, and it would appear that Chan-Tien scaling is, for present purposes, the most accurate of the three broad-band scaling approximations. But in contrast to the prior band absorptance comparisons, the present broad-band flux computations additionally require the assumption that the black-body intensity, $B_\omega(T)$, is evaluated at a single wavenumber. The consequences of this assumption have been appraised by employing the narrow-band model, and the comparisons shown in Table 9 illustrate that the differences between the broad-band model (with Chan-Tien scaling) and the line-by-line calculations, which appear within Table 8, are largely a consequence of the wavenumber invariance of $B_\omega(T)$ within the broad-band model.

Comparisons with the line-by-line flux calculations are given in Tables 10 and 11 for several existing band models. These comprise three narrow-band models; the Goody model as given by (2) and (3) with $C = 4/\pi$, the *Malkmus* [1967] model, and a version of the Elsasser model which, as employed by *Brosmer and Tien* [1985], is of the form

$$T_{\Delta\omega} = \text{erfc}\left[\frac{\sqrt{\pi}}{2}\frac{S_{\Delta\omega}m}{\Delta\omega}(1 + S_{\Delta\omega}m/\pi\bar{\gamma})^{1/2}\right] \qquad (15)$$

where erfc (x) denotes the complementary error function, and $\bar{\gamma}$ is again given by (3) with $C = 4/\pi$. With respect to broad-band CH_4 models, there are several [*Edwards and Menard*, 1964*a*; *Edwards and Balikrishnan*, 1973; *Cess and Chen*, 1975; *Donner and Ramanathan*, 1979; *Brosmer and Tien*, 1985], and the most recent of these are incorporated within the Table 10 and 11 comparisons.

Our motivation for including the Elsasser model is that *Brosmer and Tien* [1985] have recently suggested that, for CH_4, it is superior to the Goody model, a suggestion which is certainly not consistent with Tables 10 and 11. To arrive at their conclusion, Brosmer and Tien performed measurements of the spectral band absorptance (with $\Delta\omega = 32$ cm^{-1}), from which they evaluated the spectral band parameters $S_{\Delta\omega}/\Delta\omega$ and $\bar{\gamma}/\Delta\omega$ from the Elsasser and Goody models through application of a fitting procedure. Inherent in this was the assumption that $\bar{\gamma}/\Delta\omega$ is constant over the entire band. They then compared their respective Elsasser and Goody model predictions for $\bar{\gamma}/\Delta\omega$ with an independent evaluation of this quantity, from which they concluded that the Elsasser model produced the most realistic $\bar{\gamma}/\Delta\omega$ result.

TABLE 9. Comparisons of Narrow-Band Model Calculations for the Change in Infrared Flux in Which $B_\omega(T)$ is Evaluated at the Center of the Individual 5 cm^{-1} Intervals (as in Tables 6 and 7), and Alternatively at the Band Center (1306 cm^{-1})

$B_\omega(T)$ Evaluation	Flux Reduction, W/m²		
	Top	Tropopause	Surface
1.75×10^{-6} ppv			
5 cm^{-1} intervals	4.89	4.62	6.37
1306 cm^{-1}	4.99 (2.0)	4.70 (1.7)	6.48 (1.7)
1.75×10^{-6} to 3.5×10^{-6} ppv			
5 cm^{-1} intervals	1.80	1.79	2.42
1306 cm^{-1}	1.89 (5.0)	1.86 (3.9)	2.52 (4.1)

The numbers in parentheses denote the percentage error in utilizing the 1306 cm^{-1} evaluation.

TABLE 10. Comparisons of Model Calculations for the Change in Infrared Flux Due to the Presence of CH_4 With a Mixing Ratio of 1.75×10^{-6}

Model	Flux Reduction, W/m²		
	Top	Tropopause	Surface
Line-by-line	4.88	4.68	6.38
Malkmus	5.28 (8.2)	4.91 (4.9)	6.67 (4.5)
Goody	5.73 (17.4)	5.37 (14.7)	7.26 (13.8)
Elsasser	6.60 (35.2)	6.16 (31.6)	8.42 (32.0)
Donner-Ramanathan	4.89 (0.2)	4.76 (1.7)	6.73 (5.5)
Brosmer-Tien	4.22 (−13.5)	4.03 (−13.9)	5.93 (−7.1)
Cess-Chen	2.26 (−53.6)	2.21 (−52.8)	4.21 (−34.0)

Curtis-Godson scaling is used for the Malkmus, Goody and Elsasser models, while Chan-Tien scaling is employed for the Donner-Ramanathan, Brosmer-Tien and Cess-Chen models. The numbers in parentheses denote the percentage differences from the line-by-line values.

TABLE 11. Comparisons of Model Calculations for the Change in Infrared Flux Due to an Increase in CH_4 Mixing Ratio from 1.75×10^{-6} to 3.5×10^{-6}

Model	Flux Reduction, W/m²		
	Top	Tropopause	Surface
Line-by-line	1.78	1.78	2.40
Malkmus	2.01 (12.9)	1.99 (11.8)	2.62 (9.2)
Goody	2.07 (16.3)	2.07 (16.3)	2.73 (13.8)
Elsasser	2.48 (39.3)	2.47 (38.8)	3.28 (36.6)
Donner-Ramanathan	1.55 (−12.9)	1.57 (−11.8)	2.17 (−9.6)
Brosmer-Tien	1.72 (−3.4)	1.69 (−5.1)	2.44 (−1.7)
Cess-Chen	1.00 (−43.8)	1.00 (−43.8)	1.44 (−40.0)

Curtis-Godson scaling is used for the Malkmus, Goody and Elsasser models, while Chan-Tien scaling is employed for the Donner-Ramanathan, Brosmer-Tien and Cess-Chen models. The numbers in parentheses denote the percentage differences from the line-by-line values.

TABLE 12. Comparisons of Model Calculations for the Change in Infrared Flux Due to the Presence of CH_4 With a Mixing Ratio of 1.75×10^{-6}

Data Tape	Half-Width	Flux Reduction, W/m²		
		Top	Tropopause	Surface
JPL	$0.06(296/T)$	4.89	4.62	6.37
AFGL	$0.06(296/T)$	4.79	4.52	6.26
AFGL	$\gamma_A^\circ(296/T)$	4.66	4.41	6.10
AFGL	$\gamma_A^\circ(296/T)^{0.5}$	4.53	4.38	6.06

These results refer to use of the narrow-band model, and γ_A^0 denotes the 296 K line half-width from the AFGL data tape.

But their independent evaluation of $\bar{\gamma}/\Delta\omega$ contained two errors. First, they assumed $\bar{\gamma}$ to be the actual line half-width, whereas (3) produces a $\bar{\gamma}$ which is quite different from γ_{JK} even when γ_{JK} is assumed constant throughout the band. For example, employing the JPL data tape in conjunction with (3), together with $C = 4/\pi$, a wavenumber invariant γ_{JK}, and Brosmer and Tien's $\Delta\omega = 32$ cm^{-1}, we find that $\bar{\gamma}/\gamma_{JK}$ is strongly dependent upon band location, with $\bar{\gamma}/\gamma_{JK} \simeq 30$ to 200. Secondly, Brosmer and Tien interpreted $\Delta\omega$ within (22) and (15) to be the mean line spacing, rather than the interval width which is $\Delta\omega = 32$ cm^{-1} in their experiments, and subsequently they chose $\Delta\omega = 5.1$ cm^{-1} (which is actually the multiplet spacing rather than the mean line spacing). It would thus appear that Brosmer and Tien's suggestion concerning the relative merits of the Elsasser and Goody models is actually an artifact of these misinterpretations.

It may be noted from Table 10 that the Goody model produces about 10 percent greater flux reductions, for the present atmospheric CH_4 abundance, than does the Malkmus model. Since the two models yield identical weak-line and strong-line limits [e.g., *Rodgers*, 1968], whereas as previously pointed out atmospheric CH_4 is removed from either of these asymptotic limits, then the differences shown Table 10 reflect differences in the models' transitions from one limit to the other.

Similarities and differences between the Goody and Malkmus models raise another interesting point. With reference to (2) the Goody model may be rephrased as [e.g., *Goody*, 1964]

$$T_{\Delta\omega} = \exp(1 - \hat{T}_{\Delta\omega}) \tag{16}$$

where $\hat{T}_{\Delta\omega}$ represents $T_{\Delta\omega}$ in the limit of nonoverlapping lines. The Malkmus model also is of the form of (16), with a $\hat{T}_{\Delta\omega}$ which produces a different transition from weak-line to strong-line limits. But the fact that both models yield (16) as a means of accounting for line overlap does not mean that (16) constitutes a universal expression, and the Elsasser model, as given by (15), serves as a convenient case in point. With reference to (2) and (16), (15) may be written as [see also *Goody*, 1964]

$$T_{\Delta\omega} = \operatorname{erfc}\left[\frac{\sqrt{\pi}}{2}(1 - \hat{T}_{\Delta\omega})\right] \tag{17}$$

with $\hat{T}_{\Delta\omega}$ being the same as for the Goody model, but with a different line overlap formulation than for the Goody and Malkmus models. The differences between the Goody and Elsasser models, as illustrated in Tables 10 and 11, are thus solely due to the use of (16) versus (17) as a means of accounting for line overlap.

The point is that the various narrow-band models utilize differing idealized line intensity distributions, and thus the differences illustrated within Tables 10 and 11 are not surprising. Our recent experience with other trace gases indicates that such differences vary from gas to gas, and in fact may vary from band to band for a given gas. There is no universal "best" narrow-band model.

The above also emphasizes that no single physical interpretation should be placed upon our evaluation of $C = 0.753$ within (3). Although as discussed earlier one would anticipate that $C < 4/\pi$ due to coincident lines, the value of C obviously includes other effects. A similar comment applies to the present choice of $D = 1.06$ for the broad-band model given by (4).

With reference to the broad-band models, the version of the *Cess and Chen* [1975] model, which was developed for Jovian conditions, is that employed for terrestrial applications by *Hameed et al.* [1980]. The sole difference between this model and that of *Donner and Ramanathan* [1979] is in the line structure parameter β. Both models employ the old band intensity of *Burch and Williams* [1962], which is 171 cm^{-2} atm^{-1} at 296 K. To evaluate β, Cess and Chen erroneously assumed that the mean line spacing could be replaced by the multiplet spacing, contrary to the conclusions of section 2. Donner and Ramanathan, on the other hand, determined β by comparing their band model with the laboratory data of *Gryvnak et al.* [1976].

For the *Brosmer and Tien* [1985] model, the band absorptance formulation of *Edwards and Menard* [1964*a*] was utilized, and the broad-band parameters were evaluated through a fit to the laboratory data of *Burch and Williams* [1962], and of *Edwards and Menard* [1964*b*]. In contrast to a similar approach by *Edwards and Menard* [1964*b*], who utilized the same data sets and inferred a band intensity of 185 cm^{-2} atm^{-1} from their fitting procedure, Brosmer and Tien specified a value of 134 cm^{-2} atm^{-1}.

As a final point, we have used the narrow-band model as a vehicle to illustrate sensitivity to the choice of spectroscopic input data, alternatively employing the 1982 version of the AFGL data tape [*Rothman*, 1981], and renormalizing the line intensities to the same ν_4 band intensity as we employed for the JPL data tape. Table 12 illustrates that for the same half-width the choice of data tape results in only a 2 percent change in the computed fluxes, despite the fact that the AFGL tape includes only 20 percent of the lines contained on the JPL tape. Also shown are flux calculations for which (1) has been replaced by half-widths from the AFGL tape, employing the correct temperature scaling. Again the effect is small. Lastly, a common practice is to employ kinetic-theory temperature scaling ($\gamma^0 \sim 1/T^{1/2}$) when using a data tape, and as seen from Table 12 this produces very small errors.

6. CONCLUDING REMARKS

The primary point of this paper is that, employing methane as an illustrative gas, a hierarchy of mutually consistent infrared band models can be constructed, comprising line-by-line, narrow-band and broad-band models. In that atmospheric line-by-line computations do not necessitate scaling approximations, this hierarchy of band models can in turn be employed to test scaling procedures, and it has been shown that Curtis-Godson narrow-band and Chan-Tien broad-band scaling provide accurate means of accounting for atmospheric temperature and pressure variations. The general validity of this conclusion, however, might be restricted to the present use

of an altitude-invariant mixing ratio, and it should not be extrapolated to atmospheric trace gases such as ozone.

Several peculiarities were noted with respect to the application of narrow-band models (e.g., Figures 2 and 3), and it is emphasized that methane might comprise an extreme case in this regard, due both to line splitting and the presence of a Q branch.

Comparisons of the band models with laboratory data produced the best agreement when, within the band models, spurious band intensities were used which are consistent with the respective laboratory data sets, but which are not consistent with our current knowledge of the intensity of the ν_4 methane band. This emphasizes the need for improved laboratory band absorptance measurements. In particular, issues such as possible departures from a Lorentzian line shape cannot be addressed without the availability of accurate laboratory measurements.

Acknowledgments. We benefited from numerous discussions with Prasad Varanasi. This work was supported by the National Science Foundation through grant ATM8515310 and by the National Aeronautics and Space Administration through grant NSG7320.

REFERENCES

Brosmer, M. A., and C. L. Tien, Infrared radiation properties of methane at elevated temperatures, *J. Quant. Spectrosc. Radiat. Transfer, 33*, 521–532, 1985.

Burch, D. E., and D. Williams, Total absorptance of carbon monoxide and methane in the infrared, *Appl. Opt., 1*, 587–594, 1962.

Cess, R. D., and S. C. Chen, The influence of ethane and acetylene upon the thermal structure of the Jovian atmosphere, *Icarus, 26*, 444–450, 1975.

Cess, R. D., and V. Ramanathan, Radiative transfer within the atmosphere of Mars and that of Venus above the cloud deck, *J. Quant. Spectrosc. Radiat. Transfer, 12*, 933–945, 1972.

Cess, R. D., and L. S. Wang, A band absorptance formulation for nonisothermal gaseous radiation, *Int. J. Heat Mass Transfer, 13*, 547–555, 1970.

Chan, S. H., and C. L. Tien, Total band absorptance of nonisothermal infrared-radiating gases, *J. Quant. Spectrosc. Radiat. Transfer, 9*, 1261–1271, 1969.

Chedin, A., and N. A. Scott, The impact of spectroscopic parameters on the composition of the Jovian atmosphere discussed in connection with recent laboratory, earth and planetary observation programs, *J. Quant. Spectrosc. Radiat. Transfer, 32*, 453–461, 1984.

Donner, L., and V. Ramanathan, Methane and nitrous oxide: Their effects on terrestrial climate, *J. Atmos. Sci., 37*, 119–124, 1979.

Edwards, D. K., and A. Balakrishnan, Thermal radiation by combustion gases, *Int. J. Heat Mass Transfer, 16*, 25–40, 1973.

Edwards, D. K., and W. A. Menard, Comparison of models for correlation of total band absorption, *Appl. Opt., 3*, 621–625, 1964*a*.

Edwards, D. K., and W. A. Menard, Correlations for absorption by methane and carbon dioxide gases, *Appl. Opt., 3*, 847–852, 1964*b*.

Edwards, D. K., and S. J. Morizumi, Scaling of vibration-rotation band parameters for nonhomogeneous gas radiation, *J. Quant. Spectrosc. Radiat. Transfer, 10*, 175–188, 1970.

Goody, R. M., A statistical model for water vapor absorption, *Q. J. R. Meteorol. Soc., 78*, 165–169, 1952.

Goody, R. M., *Atmospheric Radiation*, 436 pp., Oxford University Press, New York, 1964.

Gryvnak, D. A., D. E. Burch, R. L. Alt, and D. K. Zgonc, Infrared absorption by CH_4, H_2O and CO_2, *Rep. AFGL-TR-76-0246*, 84 pp., Air Force Geophys. Lab., Bedford, Mass., 1976.

Hameed, S., R. D. Cess, and J. S. Hogan, Response of the global climate to changes in atmospheric chemical composition due to fossil fuel burning, *J. Geophys. Res., 85*, 7537–7545, 1980.

Kiehl, J. T., and V. Ramanathan, CO_2 radiative parameterizations used in climate models: Comparison with narrow band models and with laboratory data, *J. Geophys. Res., 88*, 5191–5202, 1983.

Malkmus, W., Random Lorentz band model with exponential tailed S^{-1} line-intensity distribution function, *J. Opt. Soc. Am., 57*, 323–329, 1967.

McClatchey, R. A., R. W. Fenn, J. E. A. Selby, F. E. Volz, and J. S. Garing, Optical properties of the atmosphere, *Rep. AFCRL-71-0279*, 85 pp., Air Force Cambridge Res. Lab., Cambridge, Mass., 1971.

Orton, G. S., and A. G. Robiette, A line parameter list for the ν_2 and ν_4 bands of $^{12}CH_4$ and $^{13}CH_4$, extended to $J' = 25$ and its application to planetary atmospheres, *J. Quant. Spectrosc. Radiat. Transfer, 24*, 81–95, 1980.

Ramanathan, V., Radiative transfer within the earth's troposphere and stratosphere: A simplified radiative-convective model, *J. Atmos. Sci., 33*, 1330–1346, 1976.

Ramanathan, V., and R. E. Dickinson, The role of stratospheric ozone in the zonal and seasonal radiative energy balance of the earth-troposphere system, *J. Atmos. Sci., 36*, 1084–1104, 1979.

Ramanathan, V., R. J. Cicerone, H. B. Singh, and J. T. Kiehl, Trace gas trends and their potential role in climate change, *J. Geophys. Res., 90*, 5547–5566, 1985.

Rodgers, C. D., Some extensions and applications of the new random model for molecular band transmission, *Q. J. R. Meteorol. Soc., 94*, 99–102, 1968.

Rodgers, C. D., and C. D. Walshaw, The computation of infrared cooling rate in planetary atmospheres, *Q. J. R. Meteorol. Soc., 92*, 67–92, 1966.

Rothman, L. S., AFGL atmospheric absorption line parameters compilation: 1980 version, *Appl. Opt., 20*, 791–795, 1981.

Varanasi, P., S. Sarangi, and L. Pugh, Measurements on the infrared lines of planetary gases at low temperatures, I, ν_3-fundamental of methane, *Astrophys. J., 179*, 977–982, 1973.

Varanasi, P., L. P. Giver, and F. P. J. Valero, Thermal infrared lines of methane broadened by nitrogen at low temperatures, *J. Quant. Spectrosc. Radiat. Transfer, 30*, 481–490, 1983.

World Meteorological Organization (WMO), Report of the meeting of experts on potential climatic effects of ozone and other minor trace gases, *WMO Global Ozone Res. Monit. Proj. Rep., 14*, 35 pp., 1982.

World Meteorological Organization (WMO), The intercomparison of radiation codes in climate models (ICRCCM), *Rep. WCP-93*, edited by Frederick M. Luther, 37 pp., Geneva, Switzerland, 1984.

J. Caldwell, R. D. Cess, and D. P. Kratz, Laboratory for Planetary Atmospheres Research, State University of New York, Stony Brook, NY 11794.

S. J. Kim, National Space Science Data Center, Code 633, NASA Goddard Space Flight Center, Greenbelt, MD 20771.

(Received November 30, 1985;
revised April 29, 1986;
accepted May 8, 1986.)